Pers Ubiquit Comput
DOI 10.1007/s00779-010-0350-4

ORIGINAL ARTICLE

The smart car seat: personalized monitoring of vital signs in automotive applications

Marian Walter · Benjamin Eilebrecht · Tobias Wartzek · Steffen Leonhardt

Received: 3 April 2010 / Accepted: 20 November 2010

Abstract Embedded wireless sensors are important components of mobile distributed computing networks, and one of the target applications areas is health care. The preservation of mobility for senior citizens is one of the key issues in maintaining an independent lifestyle. Thus health technologies inside a car can contribute both to safety issues (supervision of driver fitness) as well as healthcare issues by monitoring vitals signs imperceptibly. In this paper, three embedded measurement techniques for non-contact monitoring of vital signals have been investigated. Specifically, capacitive electrocardiogram (cECG) monitoring, mechanical movement analysis (ballistocardiogram, BCG) using piezo-foils and inductive impedance monitoring were examined regarding their potential for integration into car seats. All three sensing techniques omit the need for electroconductive contact to the human body, but require defined mechanical boundary conditions (stable distances or, in the case of BCG, frictional connection). The physical principles of operation, the specific boundary conditions regarding automotive integration and the results during wireless operation in a running car are presented. All three sensors were equipped with local intelligence by incorporating a microcontroller. To eliminate the need for additional cabling, a wireless Bluetooth communication module was added and used to transmit data to a measurement PC. Finally, preliminary results obtained during test drives on German city roads and highways are discussed.

M. Walter (✉) · B. Eilebrecht · T. Wartzek · S. Leonhardt
Philips Chair for Medical Information Technology,
RWTH Aachen University, Aachen, NRW, Germany
e-mail: walter@hia.rwth-aachen.de

Keywords Distributed sensor network · Wireless sensor · Non-contact monitoring · cECG · BCG · MIT · Automotive · Vehicle seat

1 Introduction

Research on wearable monitoring systems has attracted much attention and activities during recent years [1, 2]. It is thought that smart embedded sensing systems are one of the possible options to control future costs of health care in aging societies. The demographic changes that many countries are going to face will be accompanied by an increasing number of elderly car drivers, and thus automotive medical support is expected to attract further attention by insurances, health care providers or emergency services. Two typical use cases might be defined for such a scenario. Driver fitness monitoring is of major concern, when acute health problems impair the ability to drive safely. A car-integrated medical sensor system could be capable of detecting such critical conditions and initiate appropriate measures ranging from drive interventions (e.g. safety auto pilot) to emergency services (e.g. car to car or car to emergency communication services, qualified ambulance call). If the sensor system inside the car is able to acquire validated physiological data on a regular basis, the vital signs data can also be used in a broader context as part of a general home-health monitoring system, extending the range of coverage and connectivity.

To monitor vital signs, like electrical and mechanical heart activity as well as breathing rate, we investigated and subsequently implemented three non-contact methods, namely capacitive ECG monitoring (cECG), mechanic heart activity monitoring using ballistocardiograms (BCG), and magnetic impedance monitoring to measure mechanic

Published online: 07 January 2011

heart and breathing activity. Other methods for non-contact monitoring of vital signs also come to mind, including e.g. radar Doppler sensing. This technique was described e.g. by Geisheimer [3]. In 2009, reports on non-contact monitoring of vital signs using 2.4 and 5.8 GHz radar sensors, respectively, became available [4, 5].

Over the last decade, there have been a few reports on related issues like sensor integration, vital sign monitoring and accompanying embedded computing in public or private transportation scenarios. Vehicle seat occupation, passenger weight and size detection (for airbags) and drowsiness detection have been addressed. For example, in 1999 Voisin et al. reported about pressure sensor integration into car seats [6]. Capacitive detectors to distinguish between an empty and occupied vehicle seat were presented by Tumpold and Satz [7] in 2009. Very recently, Schumm et al. reported about integrating several non-contact vital sign monitoring techniques into passenger seats of an airplane [9]. Finally, preliminary results of capacitive ECG monitoring in a vehicle were published by our group in 2008 [8].

To the author's knowledge, the first reference on isolated electrodes for monitoring of biopotentials without conductive contact was a paper by Richardson [10]. It was soon followed by the work of David and Portnoy [11]. In the recent past, several ECG applications were reported, like contact-free ECG monitoring in bed [12, 13], on a toilet seat [14], in a bath tub [15], in office chairs [16–18] and on an incubator mattress [19]. In addition, there have been reports on non-contact electroencephalogram (EEG) measurements [20] and electromyogram (EMG) monitoring [21].

Mechanical heart activity may be detected by pressure transducers or other force sensors, preferably located in the seat, which actually measure inertial forces due to accelerated blood being sucked into the heart and traveling along the arterial tree. Such measurements are referred to as "ballistocardiograms" (BCG), see [22]. Regarding the question of possible integration, a particularly suiting design is the so called electromechanical film (EMFi) sensor. Since 2004, EMFi sensors, mostly integrated in chairs, have been used by a Finnish research group for cardiac function monitoring [23– 25].

Finally, magnetic impedance monitoring is another contact-free technique that is based on the induction of eddy currents into conductive tissues. By measuring the (very small) re-induced voltage due to these eddy currents, the (often time-varying) impedance of the underlying biological tissue can be evaluated. One of the first publications on the subject was a three-coil arrangement by Tarjan and McFee [26], with the determination of cardiac stroke-volume as the intended target application. Subsequent applications with various coil setups included in-vivo determination of heart rate [27] and lung activity [28], as well as magnetic induction imaging [29]. A recent overview of possible coil arrangements can be found in [30]. In this paper, we use a single-coil arrangement where excitation and measurement are performend with the same coil [31].

2 Methods and materials

2.1 Smart embedded sensor node

The principal design of an embedded sensor node is shown in Fig. 1. Besides one or several sensors, a node includes local computing power including analogue-to-digital conversion, filtering, signal analysis, etc. The MSP 430, a 16-bit Ultra-Low Power μC family from Texas Instruments, has been selected as a computing platform. In addition, communication was established via Bluetooth modules.

2.2 Capacitive ECG monitoring

While normal Ag/AgCl electrodes feature a (mainly) resistive behaviour, insulated electrodes form a (mainly) capacitive interface to the human body. In order to make up for the rather high coupling impedance, insulated electrodes need direct amplification close to the coupling surface (so called "active electrodes"). Also, since capacitive measurements are rather sensitive to noise, these electrodes typically need active shielding [32]. A block diagram and an equivalent circuit for the active electrode is given in Fig. 2.

Note that R_{ins} and R_{cloth} represent the resistances of the electrode insulation (approx. 20 μm of a transparent acrylic resin providing an insulating coating) and of the cloth layer, respectively, while C_{cloth} and C_{ins} stand for the (dominant) capacitive behaviour of insulation and cloth layer. In our design, the electrode coupling area was $A_{\text{ins}} = 4\ \text{cm} \times 8\ \text{cm}$. As provided by the data sheet, the insulating lacquer Plastik 70 (from CRC Industries Deutschland GmbH, Iffezheim, Germany) yields $\rho_{\text{ins}} \approx 5 \cdot 10^{16}\,\Omega\text{cm}$ and $\epsilon_r = 2.3$ [33]. Assuming a homogeneous

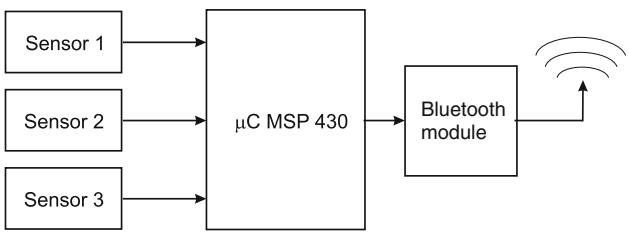

Fig. 1 Block diagram of smart wireless sensor node

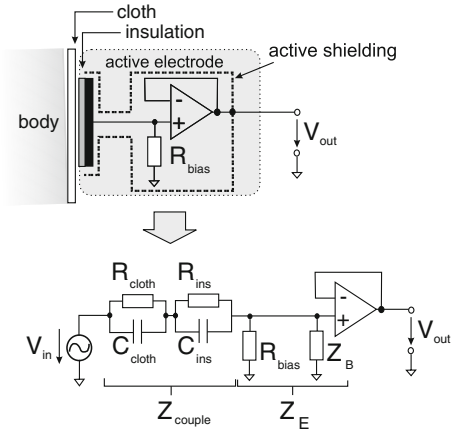

Fig. 2 Block diagram and equivalent circuit for an active electrode including an operational amplifier acting as a voltage follower and an additional bias resistor (modified from [8])

thickness of the insulating layer, R_{ins} and C_{ins} may be calculated as

$$R_{\text{ins}} = \rho_{\text{ins}} \cdot \frac{d_{\text{ins}}}{A_{\text{ins}}} = 3.125\,\text{T}\Omega \tag{1}$$

and

$$C_{\text{ins}} = \epsilon_0 \epsilon_r \cdot \frac{A_{\text{ins}}}{d_{\text{ins}}} = 3.26\,\text{nF} \tag{2}$$

with $\epsilon_0 = 8.854 \cdot 10^{-12}\,\frac{\text{As}}{\text{Vm}}$. The capacity of the cloth layer may also be relatively small: assuming a homogenous thickness of $d_{\text{cloth}} = 0.25$ mm (off-the-shelf cotton shirt), again an electrode coupling area of $A_{\text{cloth}} = 32\ \text{cm}^2$ and $\epsilon_r = 1$ (mainly air), C_{cloth} can be estimated at

$$C_{\text{cloth}} = \epsilon_0 \epsilon_r \cdot \frac{A_{\text{cloth}}}{d_{\text{cloth}}} = 113\,\text{pF}. \tag{3}$$

In reality, depending on the actual ϵ_r of the textile tissue, C_{cloth} may slightly increase. On the other hand, C_{cloth} might significantly decrease with additional cloth layers. Under normal circumstances, R_{cloth} will be rather large (several GΩ) and may thus be neglected. However, significant humidity, like e.g. strong perspiration, may reduce R_{cloth} significantly, possibly down to a few kΩ. Thus, the overall coupling impedance Z_{couple} of the electrode itself can be computed by

$$Z_{\text{couple}} = \frac{1}{\frac{1}{R_{\text{cloth}}} + j\omega C_{\text{cloth}}} + \frac{1}{\frac{1}{R_{\text{ins}}} + j\omega C_{\text{ins}}}. \tag{4}$$

While the second term is mainly capacitive and responsible for a capacitive coupling to the body, the first term may be more capacitive or resistive, depending on air humidity and transpiration. In order to have a sufficient voltage drop at the input, a high input impedance of the front end operational amplifier is required [14]. Let the input impedance of the voltage follower be denoted by Z_B. The device data sheet gives the actual value of Z_B (in our case: $10^{14}\Omega \| 3$ pF). Z_{couple} and Z_B mainly form a high pass filter (with the exact values depending on R_{cloth} and C_{cloth}, but in any case restricting the possible signal transfer at lower frequencies). On the other hand, any static charges on the coupling capacities C_{ins} and/or C_{cloth} which may have been collected from the environment need to be discharged somehow. To solve this problem, an external bias resistance was connected in parallel with Z_B. By setting $R_{\text{Bias}} = 50\,G\Omega$, a good compromise between the time required for discharging the coupling capacitance and a proper edge frequency of the high pass filter was found. Now, the overall input impedance Z_E of the operational amplifier amounts to

$$Z_E = \frac{R_{\text{bias}} \cdot Z_B}{R_{\text{bias}} + Z_B} \approx R_{\text{bias}} \tag{5}$$

and Z_{couple} and Z_E form a complex voltage divider. As is true for all biopotentials, cECG monitoring requires (at least) two active electrodes. In order to provide a potential, the two single signals must be subtracted from each other by means of a subsequent instrumental amplifier.

In practice, any environmental power source V_p (e.g. 50 Hz interferences from the power supply line), which is capacitively coupled to the patient body, causes a common mode voltage V_{CM} between the subject's body and the insulated circuit common ground [14]. Due to the limited common mode rejection ratio (CMRR) of any real world instrumental amplifier (in our case: CMRR = 115 dB), such common mode voltages cause interferences in the output signal V_{out}, see Fig. 3, and have to be suppressed as much as possible.

A second reason for trying to maximize reduction of V_{CM} is the transformation of electrode inhomogenities to a differential signal V_D at the input of the instrumental amplifier via a virtual bridge circuit, see Fig. 4.

Even in case of an infinite CMRR, any difference in coupling impedances $Z_{\text{couple},1}$ and $Z_{\text{couple},2}$, e.g. as a result of cloth inhomogeneity or difference in electrode coverage by the subject's body, is directly converted into a input difference $V_D \neq 0$, provided that $Z_{E,1} \approx Z_{E,2} = \text{const}$.

To reduce common mode effects, most conventional (conductive) ECG amplifier designs feature a so called

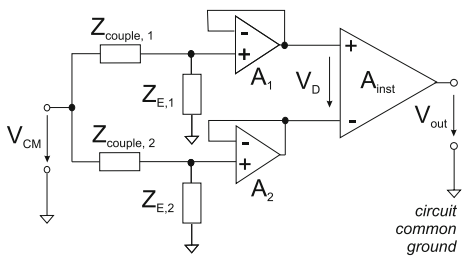

Fig. 3 Amplifier chain illustrating common mode effects (modified from [18])

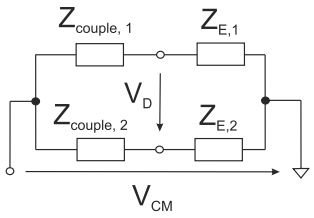

Fig. 4 Equivalent circuit to illustrate the effect of unequal electrodes causing $V_D \neq 0$ at the input of the instrumental amplifier

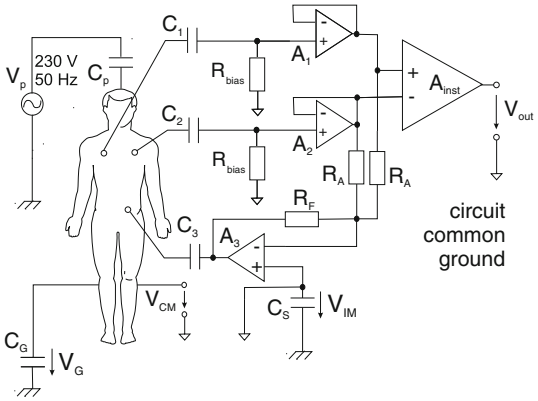

Fig. 5 Overall circuit for the driven ground plane (modified from [8])

"driven-right-leg" circuit in which any common mode voltage is actively compensated by negative feedback via an additional reference electrode [34, 35]. Expanding this concept, Kim et al. recently introduced a capacitive "driven ground plane" circuit for cECG measurements [36] which was employed in our application as well. Assuming all electrode coupling impedances to be mainly capacitive (i.e. C_1 and C_2), Fig. 5 shows the overall scenario including a virtual capacitive powerline coupling C_p and a ground coupling C_G. Note that the sum of the active electrodes' output signals is fed back via inverted amplification $-2R_F/R_A$ to a rather large insulated metal foil (C_3).

In this figure, V_{IM} represents the potential difference between floating electronic ground and earth, while V_G captures the potential between body and earth.

Note that such active cancelation techniques introduce negative feedback to the overall system. In fact, for the classical "driven-right-leg" circuit, stability was critical and required some effort to stabilize the circuit [34]. It is interesting to note that by moving from the conductive to the capacitive coupling case, stability is actually improved. A mathematical analysis of stability for this case has recently been provided [18].

2.3 Mechanical BCG monitoring

As mentioned in the introduction, the measurement of inertial forces due to blood movement and thus of mechanical heart activity is often referred to as "ballistocardiogram" (BCG). It can be detected by a capacitive sensor mat based on a quasi-piezoelectric force transducer called "EMFi sensor" ([23], available from Emfit Ltd., Vaajakoski, Finland). Figure 6 shows an equivalent circuit for the EMFi sensor and gives an example amplifier circuit.

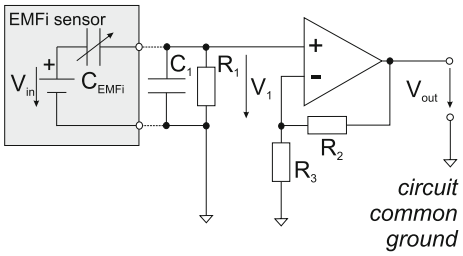

Fig. 6 Equivalent circuit of the EMFi sensor and the following voltage amplifier (as proposed by Emfit Ltd.)

By using a voltage amplifier instead of a charging amplifier, resistor R_1 is used for discharging the EMFi sensor capacitance C_{EMFi}. With a size of 35 cm × 30 cm and a capacitance of 22 pF/cm^2, the sensor capacitance amounts to 23.1 nF. According to [25], most BCG signal information is located at frequencies between 1.5 and 20 Hz. Together with R_1 (here: $R_1 = 1\,\mathrm{M\Omega}$), C_{EMFi} and $C_1 (C_1 = 100\,\mathrm{nF})$ form a high pass filter with the transfer function

$$\frac{V_1(s)}{V_{\mathrm{in}}(s)} = \frac{s \cdot R_1 \cdot C_{\mathrm{EMFi}}}{s \cdot R_1 \cdot (C_{\mathrm{EMFi}} + C_1) + 1} \tag{6}$$

and a cut-off frequency f_C of

$$f_c = \frac{1}{2\pi R_1 \cdot (C_{\mathrm{EMFi}} + C_1)} = 1.6\,\mathrm{Hz}. \tag{7}$$

The subsequent non-inverting voltage amplifier was adjusted to a gain of 40. Furthermore, a 6th order Butterworth lowpass filter with a cut-off frequency $f_{c,LP} =$ 20 Hz and a 50 Hz Notch filter with cut-off frequencies $f_L =$ 40 Hz und $f_H = 60\,\mathrm{Hz}$ were included for analogue signal processing.

2.4 Magnetic impedance monitoring

The mechanical activities of heart, diaphragm and thorax move blood and air through the body. From an electrical impedance point of view, this is a movement of well-conducting (blood) and poor-conducting (air) matter inside the chest region. By inducing eddy currents into the tissue and measuring the re-inducted field externally, these impedance changes can be monitored, see Fig. 7.

In a homogeneous tissue, eddy currents would follow a circular path. However, in any practical application these pathways will be closed, but not circular. The governing law is given by Maxwell's law

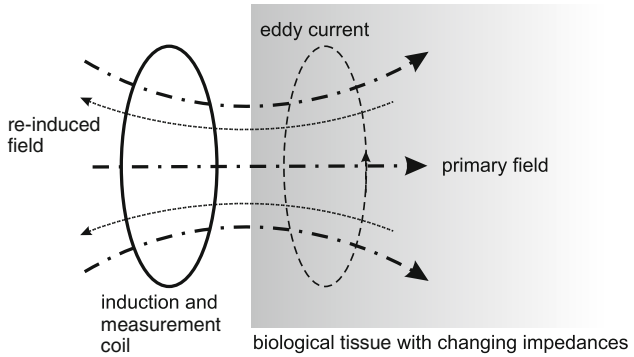

Fig. 7 Principle of re-inducted field monitoring due to flow of eddy currents inside a homogenous biological tissue

$$\nabla \times \mathbf{E} = -\frac{\mathrm{d}}{\mathrm{d}t}\mathbf{B} \tag{8}$$

and

$$\mathbf{J} = \kappa \cdot \mathbf{E}. \tag{9}$$

The resulting re-induced field **H** is proportional to the impedance distribution along the current path inside the body and can be measured as a re-induced voltage in an external coil

$$\nabla \times \mathbf{H} = \mathbf{J} + \frac{\mathrm{d}}{\mathrm{d}t}(\epsilon \cdot \mathbf{E}). \tag{10}$$

However, an exact calculation of the resulting magnetic fields would require an anatomically precise body model with identified tissue types. In addition, it would need to include the movements of heart and diaphragm. If all tissue conductivities were known, a FEM simulation based on Maxwell's Theory could be performed. Unfortunately, such an anatomical model is not yet available, but a simplified approximative model for the heart has recently been introduced [31].

In a single coil arrangement, the source magnetic field and the re-induced field **H** are superimposed. However, impedance change of $Z_{\mathrm{coil}} = R_{\mathrm{coil}} + j\omega L_{\mathrm{coil}}$ due to heart and lung activity can be monitored. As shown for a simplified heart model in [31], the coil impedance change due to heart activity is dependend on

$$\Delta Z_{\mathrm{coil}} \sim -\omega^2 \cdot L_{\mathrm{coil}} \cdot \Delta I_{\mathrm{eddy}} \tag{11}$$

and a real number. Since changes in tissue impedance directly affect I_{eddy}, the result is a change in R_{coil}. While we are not aware of any analytical model for lung tissue and ventilation-induced impedance changes therein, several experiments including our own indicate that similiar realtionships may hold for ventilation-induced tissue impedance changes. A smart way to monitor the coil impedance change is to embed it into a LC oscillator circuit. Hence, the resonance frequency is a direct function of R_{coil} and given by

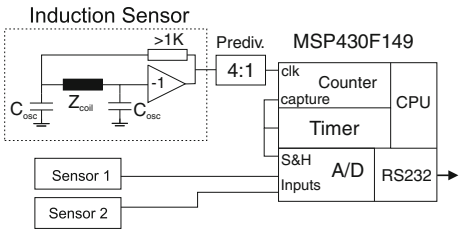

Fig. 8 Block diagram of LC oscillator circuit for single-coil monitoring of magnetic impedance changes (modified from [31])

Fig. 9 The test car, a two-seated gasoline-powered SMART^{TM}, manufactured by Mercedes-Benz Cars, Stuttgart, Germany

$$\omega_{\mathrm{res}} = 2\pi \cdot f_{\mathrm{res}} = \sqrt{\frac{1}{L_{\mathrm{coil}}C} - \frac{R_{\mathrm{coil}}^2}{2L_{\mathrm{coil}}}} \tag{12}$$

A block diagram of the monitoring circuit including external reference sensors is shown in Fig. 8.

2.5 Implementation

The different non-contact monitoring systems were integrated into original driver's and co-driver's seats of a stock-production two-seat city test car, see Fig. 9.

2.5.1 ECG sensitivity at the back

The human back is not a standard location for ECG recordings. Thus, to systematically optimise the electrode position on the human back, we studied various electrode positions and combinations, see Fig. 10. As a sensitivity marker, we measured the amplitude of the QRS complex. The results given in Table 1 indicate that a skew electrode arrangement produces higher sensitivity than a horizontal electrode placement, as originally proposed by Lim and coworkers [17] and also by our group [16, 18].

In fact, this finding is not very surprising as the typical electrial axis of the heart for the QRS complex may vary between $-30°$ and $+90°$ (with respect to the horizontal axis when frontally measured on the chest). Typical values are $30°\ldots60°$ which fits well to our back measurements.

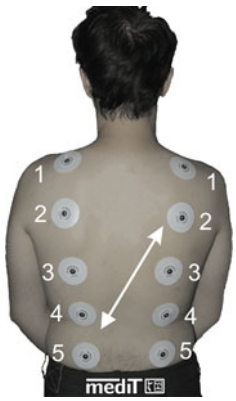

Fig. 10 Different electrode locations and combinations: the electrode pair connected by the arrow corresponds to combination 5–2 in Table 1

Table 1 QRS amplitudes for different electrode combinations

Electrode combination	QRS peak amplitude [mV]	Electrode combination	QRS peak amplitude [mV]
1–1	0.25	3–4	0.22
1–2	0.30	3–5	0.18
1–3	0.32	4–1	0.73
1–4	0.42	4–2	0.74
1–5	0.61	4–3	0.62
2–1	0.43	4–4	0.34
2–2	0.41	4–5	0.19
2–3	0.28	5–1	1.00
2–4	0.21	5–2	1.00
2–5	0.38	5–3	0.65
3–1	0.66	5–4	0.51
3–2	0.65	5–5	0.23
3–3	0.49		

2.5.2 *Instrumentation of driver's and co-driver's seat*

The driver's seat was equipped with the magnetic impedance monitoring system positioned in the backrest (Fig. 11, left). Using spacers, the coil was mechanically connected to the metal seat frame. While this is straightforward, it has the possible drawback of relative movements between coil and torso of the volunteer.

Both the capacitive ECG and the BCG monitoring sensors were integrated into a co-driver's seat and backrest. The driven ground plane was realized by a conductive textile with an area of 680 cm^2 and a clearance of 1 cm to each electrodes' surface. The active electrodes were fixed with a vertical center to center distance of 12 cm and a horizontal distance of 13 cm, respectively. The right figure in Fig. 11 illustrates the electrode placement and the driven ground plane under the covering of the backrest (cotton wool material with a thickness of 0.5 mm) of the co-driver's seat. The BCG measurement system (EMFi sensor) was integrated into the same car seat.

2.5.3 *Computing and wireless communication*

For digitalization purposes, microcontroller boards (MSP430F1612, Texas Instruments Inc., Dallas, U.S.A.) with an integrated 12-bit A/D-converter were designed. All three signals were converted with a sampling rate of 1,000 Hz and transmitted via a Bluetooth™ module (Promi-ESDTM, distributed by Hantz & Partner GmbH, Gundelfingen, Germany). At the end of the signal path, the signals were recorded by a Bluetooth™ enabled notebook PC. A LabVIEW™ application was used for data display and storage. Figure 12 gives an impression of the communication scenario.

3 Results

3.1 cECG monitoring

The cECG monitoring system was tested during different driving scenarios: motor switched off, motor running idle, driving on city roads and on the German Autobahn. During all trials, the subjects were wearing normal cotton shirts

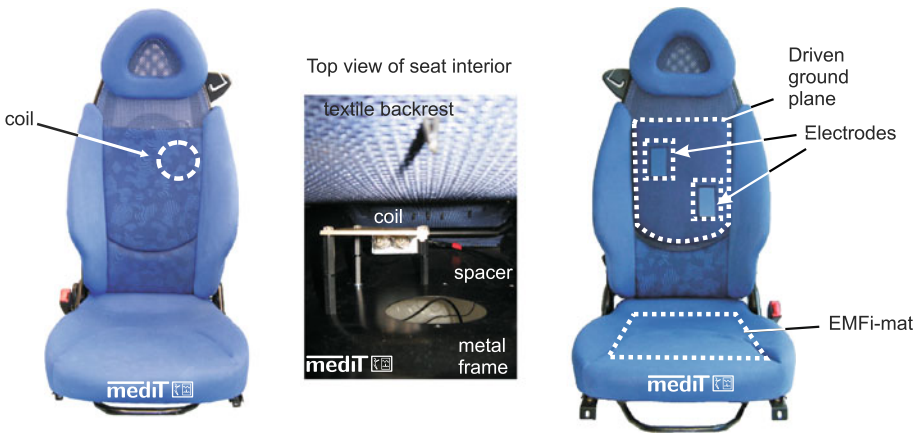

Fig. 11 The driver's seat features (*hidden*) magnetic impedance monitoring in the backrest of the seat (*left*). The center figure gives a top view of seat interior including the mechanical fixation of the coil. The co-driver's seat (*right*) features cECG monitoring in the backrest and the BCG sensor in the seat (from [8])

Fig. 12 Wireless communication via Bluetooth between co-driver's seat and PC (modified from [8])

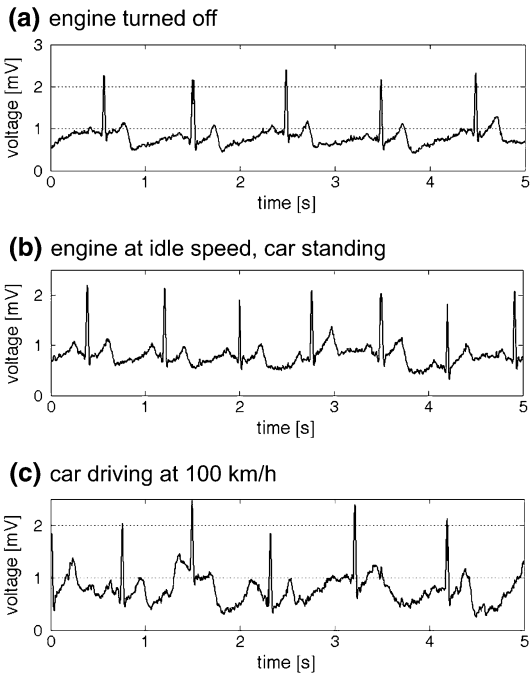

Fig. 13 cECG signal recorded from the backrest (male healthy volunteer, 27 year, sitting on the co-driver's seat, from [8])

with a thickness of 0.3 mm and cotton trousers of 1 mm thickness. All measurements were obtained under normal breathing conditions without any high-handed movements.

To give a few examples, Fig. 13 shows several cECG signals obtained with the developed system in different driving states.

In general, the cECG signal was nicely recordable from the co-driver's seat with electrodes in the backrest (a). The running motor itself did not pose a severe problem on the signal quality (b). However, the chosen test car is known for a rather stiff adjustment of shock absorbers and bumpers. As can be seen in (c), the resulting body movements on the seat caused the null line to temporarily deviate somewhat from zero. However, the QRS complex was always visible.

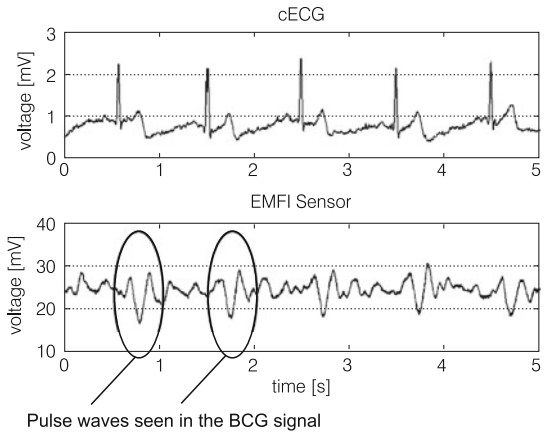

Fig. 14 EMFi signal with the engine shut down (corresponding cECG signal for comparison, both signals taken from the co-driver's seat)

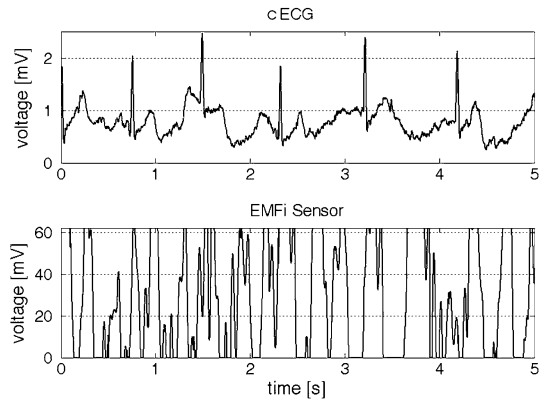

Fig. 15 EMFi signal and cECG signal during an Autobahn drive at 100 km/h (both signals taken from the co-driver's seat)

3.2 BCG monitoring

In principle, the mechanical action of the heart was visible in the BCG signal (Fig. 14). Note that this data sequence was recorded in parallel to the cECG signal already shown in Fig. 13a) which is again given for comparison. However, it must be stated that even with the engine turned off, the signal-to-noise ratio of the BCG signal was not very impressive.

When the engine was turned on, the signal got much worse, and during driving, the signal distortions were far too big to allow signal interpretation, see Fig. 15.

3.3 Magnetic impedance monitoring

The sensitivity of the magnetic impedance measurement system was first tested in the lab. Here, a healthy volunteer was placed on the chair and requested to breath into a pneumotachograph (using a difference pressure sensor type 1 Inch-D-4V 4D5-1, manufactured by All Sensors Corp.,

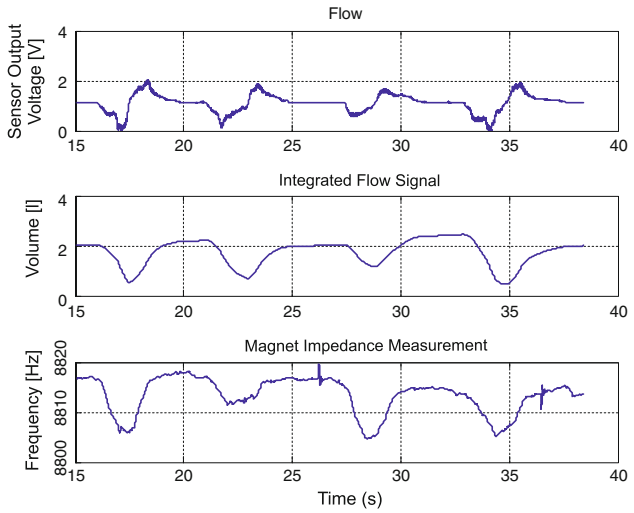

Fig. 16 Experimental lab results indicating a tight correlation between magnetic impedance and lung volume changes measured by external flow sensors

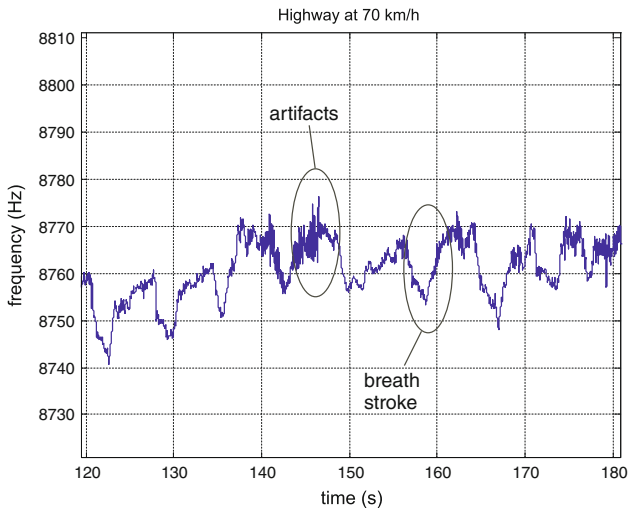

Fig. 17 frequency shift due to ventilatory impedance changes during a test drive at 70 km/h on a German Autobahn. The breathing rate was approx. 9 per minute, artifacts were present

Morgan Hill, CA 95037, USA). Some results from these experiments are given in Fig. 16.

Subsequently, the magnetic impedance signal was recorded during a second test drive on a German Autobahn. As shown in Fig. 17, individual breath strokes are clearly visible, especially with a larger tidal volume. By contrast, shallow breathing was more difficult to detect. In general, motion artifacts were present throughout the drive, especially on uneven parts of the road.

In the future, the major challenge will be to deal with motion artifacts, either by smart filtering and/or by using sensor information from additional sources for compensation. It seems especially challenging to distinguish voluntary motion from body motion introduced by shocks from the road.

4 Conclusion

A concept for an automotive wireless sensor system has been presented. Apart from the sensors, a node concept featuring a low-power microcontroller for front-end signal processing and a Bluetooth-based signal transmission has been established. Since the need for wireless signal transmission inside a vehicle may not be directly obvious, it must be stated that this could be an enormous implementation advantage, as many modern vehicle seats face difficulties in providing extra cable lines.

With the presented non-contacting heart function monitoring concept, a vehicle passenger's cECG and BCG signal could be measured simultaneously. However, without further signal processing, the BCG signal could only be identified under the condition of a standing car with turned-of engine. The ECG signal, measured by insulated electrodes at the backrest of the car seat, remained stable after approx. 250 seconds and could be detected in a standing car position as well as with different velocities. The recorded baseline shift during the first 250 s could be an effect of changing contact impedances due to a changing humidity of the clothes. Another reason could be a changing decreasing distance between the body and the electrodes' surface due to a time related compression of the cloth layer. In non-contact biopotential sensing, the signal's quality is depending on the clothes thickness [18, 20, 21] and pressure [21]. A decreasing signal quality over time was observed in [20]. However, in this work, textile electrodes with no additional insulating layer were used. As shown in our results, a cotton wool T-shirt of 0.3 mm thickness provides an adequate condition for non-contact ECG measurements through clothes. However, especially in automotive applications, motion artifacts caused by sudden accelerations and the resulting change of distance between one or both electrode surfaces and the subjects body are an method-inherent problem and remain difficult to solve.

The presented magnetic impedance measurement system was able to detect ventilation rate during driving. In our design, the coil was fixed inside the chair. As a result, there was a rather large distance between coil and body, and it can be assumed that a shorter distance would be beneficial for the signal to noise ratio. In principle, for ventilation montoring the backrest may not be an optimal location as large back muscles or the scapula could attenuate the magnetic field. Similiar to capacitive ECG recordings, motion artifacts pose a severe challenge on the technique.

Our results may easily be transferred to other areas of embedded operator supervision including military applications (monitoring of fighter pilots, tank and truck drivers, etc.), civilian aircraft applications (monitoring of pilots or

passengers), ICU applications (reducing cable connections in patient monitoring) and personal health care applications (monitoring of senior citizens at home).

References

1. Yang G-Z (eds) (2006) Body sensor networks. Springer, London
2. Pantelopoulos A, Bourbakis NG (2010) A survey on wearable sensor-based systems for health monitoring and prognosis. IEEE Tran Syst Man Cybern C Appl Rev 40(1):1–12
3. Geisheimer J (1999) RVSM [radar vital signs monitor]. IEEE Poten 17(5):21–24, Dec. 1998/Jan
4. Ichapurapu R, Jain S, John G, Monday T, Lie DYC, Banister R, Griswold J (2009) A 2.4 GHz non-contact biosensor system for continuous vital-signs monitoring.10th Annual IEEE wireless and microwave technology conference (WAMICON '09), 20–21 April
5. Li C, Yu X, Li D, Ran L, Lin J (2009) Software configurable 5.8 GHz radar sensor receiver chip in 0.13 μm CMOS for non-contact vital sign detection. IEEE radio frequency integrated circuits symposium (IEEE RFIC 2009), Boston, Massachusetts, USA, 7–9 June
6. Voisin A, Bombardier S, Levrat E, Bremont J (1998) Sensory features measurement of the under-thigh length of car seat. IEEE world congress on computational intelligence, Anchorage, Alaska, USA, 4–9 May
7. Tumpold D, Satz A (2009) Contactless seat occupation detection system based on electric field sensing. 35th Annual conference of IEEE industrial electronics (IECON '09), Porto, Portugal, 3–5 Nov
8. Leonhardt S, Aleksandrowicz A (2008) Non-contact ECG monitoring for automotive application. 5th International workshop on wearable and implantable body sensor networks (BSN 2008), The Chinese University of Hong Kong, HKSAR, China, 1–3 June
9. Schumm J, Setz C, Bächlin M, Bächler M, Arnrich B, Tröster G (2010) Unobtrusive physiological monitoring in an airplane seat. Personal and ubiquitous computing. doi:10.1007/s00779-009-0272-1, Online First™
10. Richardson PC (1967) The insulated electrode. 20th Annual conference on engineering in medicine and biology, Boston, MA, USA
11. David RM, Portnoy WM (1972) Insulated electrocardiogram electrodes. Med Biol Eng Comput 10:742–751
12. Ishijima M (1993) Monitoring of electrocardiograms in bed without utilizing body surface electrodes. IEEE Trans Biomed Eng 40(6):593–594
13. Lim YG, Kim KK, Park KS (2007) ECG recording on a bed during sleep without direct skin-contact. IEEE Trans Biomed Eng 54(4):718–725
14. Kim KK, Lim YK, Park KS (2004) The electrically non-contacting ECG measurement on the toilet seat using the capacitivly-coupled insulated electrodes. 26th EMBS conference, San Francisco, CA, USA
15. Lim YK, Kim KK, Park KS (2004) ECG measurement in the bathtub using the insulated electrodes. 26th IEEE EMBS conference, San Francisco, CA, USA
16. Leonhardt S, Aleksandrowicz A, Steffen M (2006) Magnetic and capacitive monitoring of heart and lung activity example for personal healthcare. 3rd IEEE-EMBS international summer school and symposium on medical devices and biosensors, MIT, Boston, USA, 4–6 Sep
17. Lim YG, Kim KK, Park KS (2006) ECG measurement on a chair without conductive contact. IEEE Trans Biomed Eng 53(5):956–959
18. Aleksandrowicz A, Walter M, Leonhardt S (2007) Ein kabelfreies, kapazitiv gekoppeltes EKG-messsystem (wireless ECG measurement system with capacitive coupling, in German). Biomed Technik 52:185–192
19. Kato T, Ueno A, Kataoka S, Hoshino H, Ishiyama Y (2006) An application of capacitive electrodes for detecting electrocardiogram of neonates and infants. 28th IEEE EMBS conference, New York City, USA
20. Harland CJ, Clark TD, Prance RJ (2002) Remote detection of human electroencephalograms using ultrahigh input impedance electric potential sensors. Appl Phys Let 81(17):3284–3286
21. Gourmelon L, Langereis G (2006) Contactless sensors for surface electromyography. 28th IEEE EMBS conference, New York City, USA, Aug. 30–Sept. 3
22. http://www.upscale.utoronto.ca/GeneralInterest/Harrison/BCG/BCG.html. Visited: 12 July 2008
23. Koivistoinen T, Junnila S, Värri A, Kööbi T (2004) A new method for measuring the ballistocardiogram using EMFi sensors in a normal chair. 26th IEEE EMBS conference, San Francisco, CA, USA
24. Akhbardeh A, Junnila S, Koivuluoma M, Koivistoinen T, Värri A (2005) The heart disease diagnosting system based on force sensitive chair's measurement—biorthogonal wavelets and neural networks. 2005 IEEE/ASME international conference on advanced intelligent mechatronics, Monterey, CA, USA, 24–28 July
25. Junnila S, Akhbardeh A, Barna LC, Defee I, Värri A (2006) A wireless ballistocardiographic chair. 28th IEEE EMBS conference, New York, USA, pp 5932–5935, Aug. 30–Sept. 3
26. Tarjan PP, McFee R (1968) Electrodeless measurements of the effective resistivity of the human torso and head by magnetic induction. IEEE Trans Biomed Eng 15:266–278
27. Guardo R, Charron G, Goussard Y, Savard P (1995) Contactless recordings of cardiac related thoracic conductivity changes. 17th IEEE EMBS conference, Montreal, Canada, pp 1581–1582, Sept
28. Richer A, Adler A (2005) Eddy current based flexible sensor for contactless measurement of breathing. Instrumentation and measurement techniques conference (IMTC), Ottawa, Canada, 17–19 May
29. Scharfetter H, Lackner HK, Rosell J (2001) Magnetic induction tomography: hardware for multi-frequency measurements in biological tissues. Physiol Meas 22:131–146
30. Igney C, Jäschke S, Pinter R, Waffenschmidt E, Mühlsteff J, Brauers A, Such O (2006) Planar magnetic induction impedance measurement in medicine: principles and applications. Technische Mitteilungen des Haus der Technik e.V., Essen, Germany, 99(1/2):24–30
31. Steffen M, Aleksandrowicz A, Leonhardt S (2007) Mobile non-contact monitoring of heart and lung activity. IEEE Trans Biomed Circuits Syst 1(4):250–257
32. Prance RJ, Debray A, Clark TD, Prance H, Nock M, Harland CJ, Clippingdale AJ (2000) An ultra-low-noise electrical-potential probe for human-body scanning. Meas Sci Technol 11:291–297
33. http://www.crcind.com/wwwcrc/tds/TKC3%20PLASTIK70.PDF, Visited: 2nd Dec 2010
34. Winter BB, Webster JG (1983) Reduction of interference due to common mode voltage in biopotential amplifiers. IEEE Trans Biomed Eng 30(1):58–61
35. Winter BB, Webster JG (1983) Driven-right-leg circuit design. IEEE Trans Biomed Eng 30(1):62–65
36. Kim KK, Lim YK, Park KS (2005) Common mode noise cancellation for electrically non-contact ECG measurement system on a chair. 27th annual IEEE EMBS conference, Shanghai, China
37. Searle A, Kirkup L (2000) A direct comparison of wet, dry and insulating bioelectric recording electrodes. Physiol Meas 21:271–283